Theoretical study of dissociative recombination of Cl_2^+

Mingwu Zhang,[1,2,3] Xiaohong Cai,[1] Åsa Larson,[3,*] and Ann E. Orel[4]

[1]*Institute of Modern Physics, Chinese Academy of Sciences, Lanzhou 730000, China*

[2]*Graduate School of Chinese Academy of Sciences, Beijing 100039, China*

[3]*Department of Physics, Stockholm University, S-106 91 Stockholm, Sweden*

[4]*Department of Chemical Engineering and Materials Science, University of California at Davis, Davis, California 95616, USA*

(Received 2 March 2011; revised manuscript received 31 August 2011; published 8 November 2011)

Theoretical studies of low-energy electron collisions with Cl_2^+ leading to direct dissociative recombination are presented. The relevant potential energy curves and autoionization widths are calculated by combining electron scattering calculations using the complex Kohn variational method with multireference configuration interaction structure calculations. The dynamics on the four lowest resonant states of all symmetries is studied by the solution of a driven Schrödinger equation. The thermal rate coefficient for dissociative recombination of Cl_2^+ is calculated and the influence on the thermal rate coefficient from vibrational excited target ions is investigated.

DOI: 10.1103/PhysRevA.84.052707 PACS number(s): 34.80.Ht, 31.50.Df, 34.80.Lx, 31.15.xv

I. INTRODUCTION

Dissociative recombination (DR) is a process where an electron recombines with a molecular ion to form a repulsive excited neutral state that dissociates into fragments. This process has received substantial attention by theorists and experimentalists [1]. The relevant reactions play crucial roles in the formation of many important molecules found in the interstellar medium and planetary atmospheres, and they are also important processes in a wide range of plasma environments. Knowledge of the cross sections for these reactions is crucial in producing accurate numerical models for industrially important plasma processes.

The chlorine molecule (Cl_2) is widely used in plasma processes [2] and in excimer lasers [3]. It is also of atmospheric and environmental interest [4–6]. In these media, electron collisions with chlorine molecules and molecular ions leading to dissociation are believed to play a key role. An early attempt to summarize low-energy electron-impact cross-section data for Cl_2^+ was published by Morgan [7]. A comprehensive review of current available data on electron interactions with chlorine molecules was later given by Christophorou and Olthoff [8]. A recent survey on the characteristic and modeling of chlorine high-density plasmas was made by Margot [9]. To our knowledge, there has been no theoretical nor experimental investigations of the cross section and rate coefficient for low-energy electron collisions with Cl_2^+ leading to dissociative recombination. Rather, in the modeling of chlorine plasmas, the rate coefficient of this reaction is estimated using the rate coefficients of other elements [10].

The purpose of this paper is to present results of a theoretical study of the direct mechanism of DR of Cl_2^+. Potential energy curves and autoionization widths are computed by combining structure calculations with electron scattering calculations. No spin-orbit interactions nor electronic couplings between the neutral states are included in the calculation. Rather, it is assumed that when the electron is captured into a resonant state, either autoionization (where the electron is re-emitted) or a direct dissociation into neutral fragments occurs. The method to compute the potential energy curves and widths is outlined in Sec. II. In Section III, we describe the theoretical approach to study the dynamics by solving a driven Schrödinger equation. The results are summarized in Sec. IV, including the relevant potential energy curves and the calculated cross section for DR for ground and vibrationally excited Cl_2^+ ions. In addition, the cross section is convolved with an isotropic Maxwell-Boltzmann velocity distribution for the electrons, in order to compute a thermal rate coefficient. Unless otherwise stated, atomic units are used throughout the paper.

II. POTENTIAL ENERGY CURVES AND AUTOIONIZATION WIDTHS

In this study, only the direct process of DR is investigated, which implies that no interactions between Rydberg states and resonant states are considered. It is critical in such calculations to have an accurate representation of the potential energy curves and autoionization widths that treats both the electronically bound as well as the resonant states in a balanced fashion. We have done this by combining *ab initio* structure calculations with *ab initio* electron scattering calculations. For the structure calculations, we used the multireference configuration interaction (MRCI) wave functions to determine the electronic bound adiabatic states situated below the ground state of the Cl_2^+ ion. The scattering and the structure calculations were performed at the same level in order to have a balanced representation.

In both cases, the initial molecular orbitals were obtained from a self-consistent field calculation (SCF) using a contracted $(13s11p2d/6s6p2d)$ basis set for Cl by McLean [11] augmented with one extra p orbital and one extra d orbital. Natural orbitals are determined by performing an MRCI calculation on the ground state $(X^2\Pi_g)$ of the Cl_2^+ ion. In this calculation the 10 lowest molecular orbitals, composed of the $1s$, $2s$, and $2p$ atomic orbitals are kept doubly occupied. The reference space consists of excitations of the outer 13 electrons among 8 orbitals $[(4\sigma_g)(4\sigma_u)(2\pi_u)(5\sigma_g)(2\pi_g)(5\sigma_u)]$. Single excitations out of all the reference configurations are included. The averaged natural orbitals of the degenerate components of the ground state of the ion are computed and then further

*aasal@fysik.su.se

expanded by adding $(2d)$ functions on the Cl atoms and $(4s,3p)$ functions in the center between the two atoms. These diffuse functions are needed to have a good description of the Rydberg states and the ionization continuum.

Finally, the MRCI calculations on the Cl_2^+ and Cl_2 systems are performed using the natural orbitals and the same reference space as described above. Single external excitations are included for the neutral system. The calculations are carried out in C_{2v} symmetry. For all irreducible representations, the lowest 30 roots are computed. Note that these states contain not only the doubly excited states relevant for the direct mechanism of DR, but also Rydberg states as well as states that represent the ionization continuum. These latter states have the same character as the ground state of the ion plus an extra electron in a diffuse orbital and they can be removed from the calculations by examining the CI coefficients. The calculations are carried out for the internuclear distance in the range $3.0a_0 \leqslant R \leqslant 5.0a_0$.

For energies larger than the ground state of the ion, the doubly excited states become electronic resonant states. The potential energies as well as the autoionization widths of the resonant states are determined by performing electron scattering calculations with the complex Kohn variational method [12]. The same MRCI wave function for the target ion used in the structure calculations is employed in the scattering calculation. The scattering wave function of the neutral system is expanded and separated into the P-space and Q-space portions of the wave function, where the P-space describes the target ion and a free electron. It runs over all open states of the target ion. Here, two roots of the target ion (corresponding to the degenerate $X^2\Pi_g$ ground state) are included. The Q-space portion of the wave function is used to describe the short-range correlations and the effects of closed channels and also contains information of the resonant portion of the scattering wave function (for more details see Refs. [12,13]). The energy position and autoionization width of the resonant state are determined by performing a fit of the eigenphase sum of the T matrix to a Breit-Wigner form [14].

In these calculations we ignore spin-orbit effects. The molecular states are labeled with the ${}^{(2S+1)}\Lambda_{(g/u)}$ term symbol. In order to obtain the relevant quasidiabatic potential curves we identify the character of the resonant states by comparing the energies obtained with the structure and scattering calculations. If the resonant states are narrow Feshbach resonances dominated by doubly excited configurations, they can easily be separated from the states dominated by singly excited configurations describing Rydberg states or the ionization continuum. The quasidiabatic states are constructed by removing the states with configurations dominated by single excitations.

III. REACTION DYNAMICS

The reaction dynamics on the quasidiabatic resonant states is investigated by using a time-independent approach where a driven Schrödinger equation is solved [15]

$$\left[E + \frac{1}{2\mu}\frac{\partial^2}{\partial R^2} - \hat{V}_i(R)\right]\xi_i(R) = \sqrt{\frac{\Gamma_i(R)}{2\pi}}\chi_{v_0}(R). \quad (1)$$

Here the right-hand side of the equation corresponds to the "entry amplitude" and is composed of the nuclear wave function of the target ion (χ_{v_0}) dressed by the electronic coupling between the ionization continuum and the resonant state that is obtained from the autoionization width Γ_i. In the so-called local or "boomerang model" [16], the potential of the resonant state is given by

$$\hat{V}_i(R) = E_i(R) - i\frac{\Gamma_i(R)}{2}. \quad (2)$$

This approximation is valid when the total energy of the system is high enough for autoionization into a complete set of vibrational levels is possible. When this is not the case, the nonlocal expression for the resonant states must be used [17]:

$$\hat{V}_i\xi_i = E_i\xi_i - i\pi\sqrt{\frac{\Gamma_i}{2\pi}}\sum_v \langle\chi_v|\sqrt{\frac{\Gamma_i}{2\pi}}|\xi_i\rangle\chi_v. \quad (3)$$

where the summation is over energetically open vibrational states of the target ion.

In order to solve the driven Schrödinger equation numerically, a finite-element method employing a discrete variable representation combined with exterior complex scaling [18,19] is used. The driven Schrödinger equation (1) is integrated out to the asymptotic region where the radial grid becomes complex. Here an asymptotic distance of $R_a = 10a_0$ is used. From the asymptotic wave function, the cross section for dissociation along state i can be computed [20]:

$$\sigma_i(E) = \frac{\pi^2 K_i}{\mu E} g_i\,|\xi_i(R_a)|^2\,. \quad (4)$$

Here g_i is the multiplicity ratio of the neutral resonant state to the ionization continuum. $K_i = \sqrt{2\mu[E - E_i(R_a)]}$ is the wave number of the asymptotic fragments and E is the collision energy. The total cross section is given by a sum of all resonant states:

$$\sigma(E) = \sum_i \sigma_i(E). \quad (5)$$

For the modeling of the chlorine plasmas a more useful quantity is the DR thermal rate coefficient. The thermal rate coefficient is obtained by convoluting the cross section with an isotropic velocity distribution of the electrons

$$\alpha(T_e) = \frac{8\pi m_e}{(2\pi m_e k T_e)^{3/2}}\int E\sigma(E)\exp\left(-\frac{E}{kT_e}\right)dE. \quad (6)$$

In Eq. (6) SI units are used. Here, k is the Boltzmann constant and m_e is the electron mass.

IV. RESULTS AND DISCUSSION

A. Potential energy curves and autoionization widths

We start by comparing the computed adiabatic potential curves of the electronically bound states of Cl_2 with potentials obtained in other theoretical studies. As mentioned above, the spin-orbit interactions are here neglected and the $\Lambda - S$ states are investigated. Peyerimhoff and Buenker [21] have performed multireference configuration interaction calculations including single- and double-excitations (MRD-CI) with a large basis set. Special emphasis was placed upon treatment of the Rydberg-valence mixing. Also, the potential

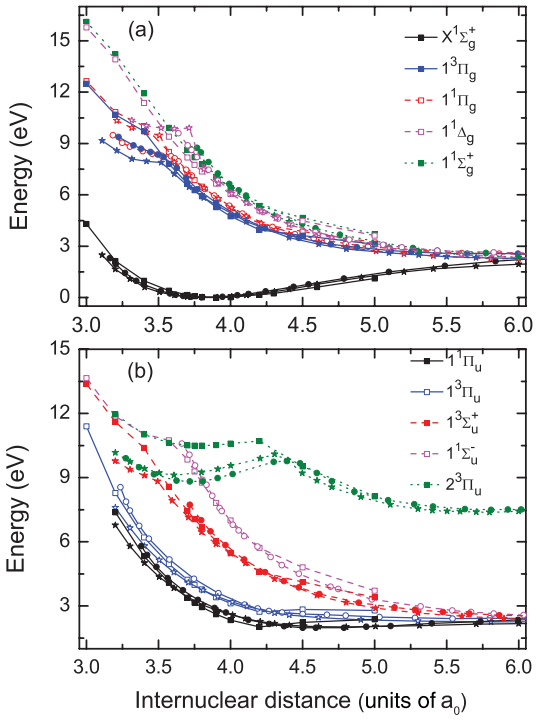

FIG. 1. (Color online) Singlet and triplet adiabatic potential curves of Cl_2 of (a) gerade and (b) ungerade symmetries. The energy scale is relative to the minimum of the $X^1\Sigma_g^+$ ground state.

curves of the positive and negative ions as well as ion-pair states were obtained. In a more recent study, Kokh *et al.* [22] have also performed MRD-CI calculations where the focus was on the low-lying ion-pair states of Cl_2. In this study, the spin-orbit interactions were considered. In Fig. 1, the singlet and triplet adiabatic potential curves of gerade [in Fig. 1(a)] and ungerade [in Fig. 1(b)] symmetries are shown. The energy of the minimum of the $X^1\Sigma_g^+$ ground state is put to zero. The potential curves computed in the present study are displayed with square symbols while the potentials of Peyerimhoff *et al.* [21] have circles and the curves of Kokh *et al.* [22] have stars. We note that, for the lower-valence states there is good agreement between our potential curves and those obtained in the other studies. However, for some of the states, especially those states that adiabatically obtain a Rydberg character at small distances, our potential curves are higher in energy compared to those obtained in the other calculations. This can be explained by the fact that our ion-potential curve is higher in energy relative to the neutral ground state. We obtain an ionization energy of about 13.0 eV instead of the 11.48 eV ionization potential obtained by Peyerimhoff *et al.* The shape of our ion-potential, however, is very similar to the one calculated by Peyerimhoff.

As mentioned above, when studying the electron capture of the Cl_2^+ ion, it is important to describe the ionization continuum and the relevant neutral bound states in a balanced fashion. The electron scattering calculations limit the number of configurations we can include in the CI calculations. In order to obtain a compact representation of the orbitals for the ionization continuum and the Rydberg states, natural orbitals of the ground state of the ion are used. The goal of this project is not to obtain good potential curves of the low-lying valence states. Rather, it is important to have sufficiently good curves for the ion and the resonant states crossing the ions. These are the electronic states that play an important role in dissociative recombination.

The four lowest quasidiabatic resonant states of Cl_2 of all the symmetries are displayed in Fig. 2. As mentioned above, the resonant states are obtained by combining the results from the electron scattering calculations above the ion with the potential curves obtained by following the configurations of the resonant states in the structure calculations below the ion. Also the potential of the ionic ground state $X^2\Pi_g$ is shown in the figure with a thicker curve. The energy-scale in Fig. 2 is relative to the minimum of the ion potential. In the direct mechanism of dissociative recombination, the reaction is driven by a capture into an electronic resonant state followed by a direct dissociation. Those electronic states of Cl_2 that cross the ion potential close to its equilibrium geometry might be important for the reaction. To obtain a sizable cross section, also the autoionization width has to be large. As can be seen in Fig. 2, there are several states that cross the ion potential close to its minimum such as the $2^1\Pi_g$, $1^1\Pi_u$, $1^1\Delta_u$, $2^3\Sigma_g^-$, and $2^3\Pi_u$ resonant states.

There are some potential curves that cross the ion at smaller distances than the equilibrium geometry. These will contribute to the low-energy cross section, but since the falloff of the Franck-Condon factors between the initial vibrational state of the target ion and the continuum wave function of the resonant state, the magnitudes of the cross sections for these states will be small.

At large energies, the electron can capture into a manifold of resonant states. These states will cross the ion potential at larger internuclear distances. These resonant states will contribute to the high-energy (> a few eV) cross section. In the present study we only include the four lowest resonant states of all symmetries.

As described above, the resonant states of Cl_2 are extracted by removing the singly excited configurations describing the ionization continuum of the Rydberg states. If we take a closer look at, for example, the resonant states of $^1\Pi_g$ symmetry (see Fig. 3), we note that the resonant states show indications of avoided crossings. The structure calculations show that the resonant states change character around these avoided crossings. There is a strongly repulsive state that will interact with less repulsive states. Similar interactions between resonant states have now been observed for a number of molecular systems such as H_3^+ [23] and HCO^+ [24]. The resonant states are only diabatized relative to the Rydberg manifold lying below the ion, not diabatized among each other. No electronic couplings between the neutral states are included in the present study. Using the direct mechanism of dissociative recombination, with no coupling, we can calculate the magnitude of the cross section but not the final state of distributions of the fragments. Resonant structures in the cross section can occur when the electronic couplings between the neutral states are added to the model [25]. When the direct mechanism is strong, the inclusion of nonadiabatic interactions between the Rydberg states or to the ionization continuum and hence the inclusion of the so-called indirect mechanism will in general cause sharp

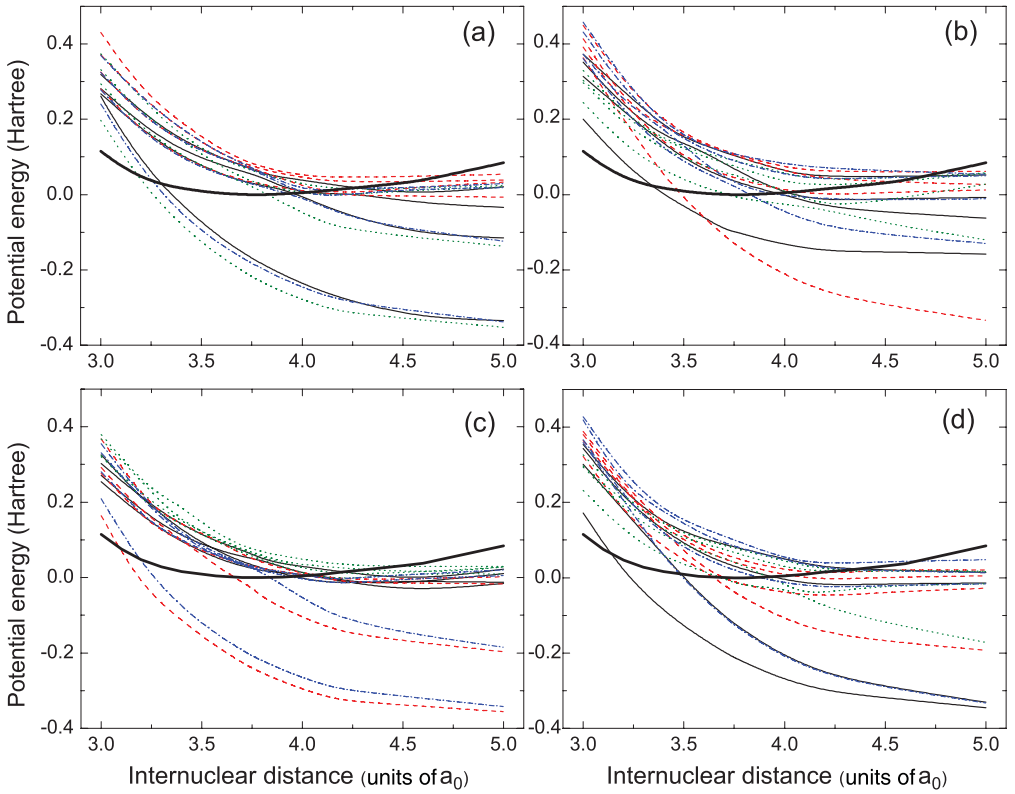

FIG. 2. (Color online) Quasidiabatic resonant states of Cl_2 of (a) singlet gerade, (b) singlet ungerade, (c) triplet gerade, and (d) triplet ungerade symmetries. The potential curve of the ground state of the ion is shown with the thick (black) curve. The energy scale is relative to the minimum of the ion. The solid (black) curves are states of Σ^+ symmetry, the dashed (red) curves correspond to Σ^- states, while dotted (green) and dotted-dashed (blue) curves show states of Π and Δ symmetries respectively.

resonant structures in the cross section and will not change its overall magnitude [26]. We neglect these nonadiabatic interactions.

From the electron scattering calculations the autoionization widths of the resonant states are obtained. In Fig. 4 the autoionization widths of some of the more important resonant states are displayed. The autoionization widths are splined between the computed points marked with symbols in Fig. 4. The resonant states participating in avoided crossings will change magnitudes of the autoionization widths when going through the avoided crossings. When the resonant state has crossed the ion potential, the autoionization width is put to

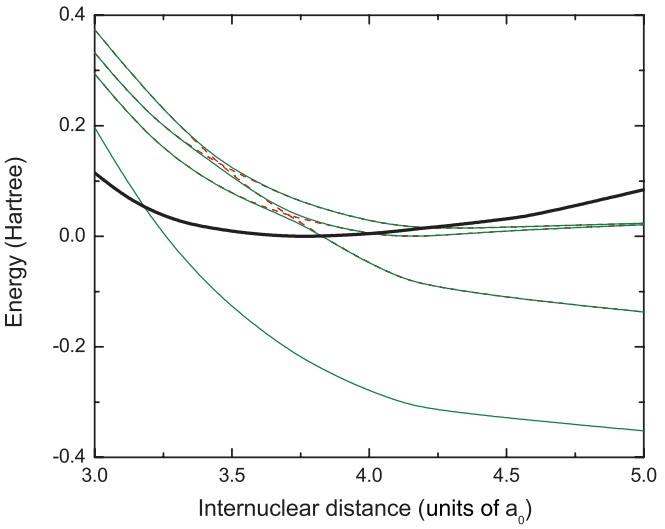

FIG. 3. (Color online) The resonant states of $^1\Pi_g$ symmetry show indications of avoided crossings. The diabatized resonant states are shown with the (red) dashed curves.

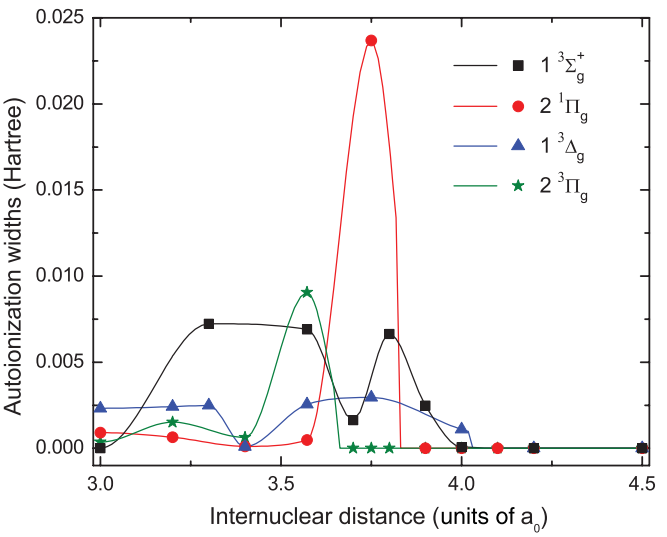

FIG. 4. (Color online) Autoionization widths of some of the most important resonant states of Cl_2.

zero indicating that autoionization is no longer energetically possible.

In $^1\Pi_g$ symmetry, electron scattering calculations reveal there is a quite broad resonant state that does not match any roots from the structure calculations dominated by doubly excited configurations. Rather, this resonant state matches a root with single excitations and is believed to be a shape resonance formed in the electron-ion scattering. This resonant state, however, has a potential curve parallel to the ion and in the direct mechanism of DR it is not open for dissociation. Hence this resonant state is not included in the present study of the dynamics.

B. Cross section

The cross section for the direct mechanism of DR of Cl_2^+ is computed by numerically solving the driven Schrödinger equation as described in Sec. III. The nonlocal model for inclusion of autoionization out of the resonant states is applied. The total cross section is obtained by summarizing the cross section from 64 resonant states. We start here by examining the cross section for electron recombination with the ion in the ground $v_0 = 0$ vibrational state. In Fig. 5 the contributions to the cross section from the resonant states of different symmetries are displayed. We note that the total cross section is about 7.2×10^{-15} cm^2 at an energy of 0.01 eV. This is a sizable cross section for a diatomic molecule. It then falls off like E^{-1} until 0.1 eV which is in accordance to the Wigner threshold law [27] for the direct mechanism of DR. Centered around 0.6 eV there is a "high-energy peak" in the cross section. The triangular peaks in Fig. 5 near 0.1 eV both in cross sections of $^3\Sigma_u^+$ and $^3\Sigma_u^-$ originate from the resonances in these states. Since the cross section is calculated on an equidistant energy grid (with $\delta E = 0.01$ eV) and these resonances occur at relative low energy, we do not have enough energy points to fully resolve the structures. However, the cross sections from these states are small relative to the total DR cross section.

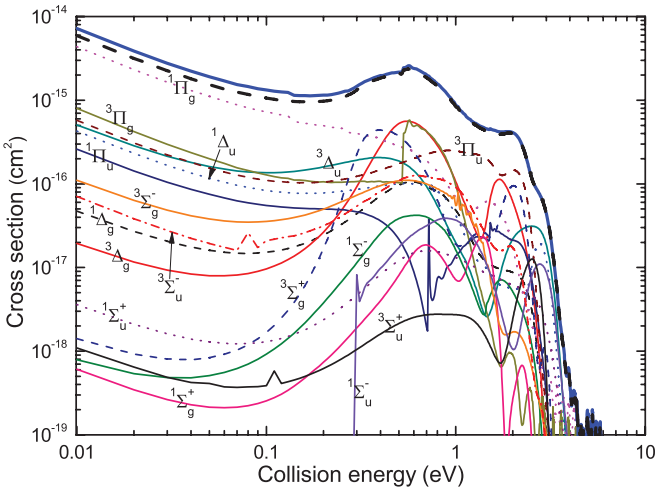

FIG. 5. (Color online) Cross section for direct DR of $Cl_2^+(v_0 = 0)$. The total cross section calculated with the nonlocal model is the thick solid (blue) curve, while the thick dashed (black) curve is the total cross section obtained by the local model. The contributions from the resonant molecular states of different symmetries are displayed with the thinner curves.

We note that it is the $2^1\Pi_g$ resonant state that contribute most to the low-energy cross section. This is one of the resonant states that cross the ion potential close to its minimum. Also this resonant state has a relative large autoionization width. This state contributes with about 61% of the total cross section at an energy of 0.01 eV. Other states that contribute to the low-energy cross section are the $2^3\Pi_g$, $2^3\Pi_u$, and $2^3\Delta_u$ resonant states.

If an electronic state crosses the ion close to its minimum, autoionization is energetically possible into only a few vibrational states of Cl_2^+ and the local approximation for treating autoionization may fail. In these cases, the inclusion of autoionization must be done using the nonlocal operator described with Eq. (3). In order to test this effect the cross section for dissociation for all resonant states were computed using both the local and the nonlocal formalism. As can be seen in Fig. 5, the total cross section with the nonlocal model is slightly higher than the total cross section computed with the local model at low collision energies. Above about 0.2 eV the two total cross sections are the same. The $2^1\Pi_g$ resonant state which has the largest cross section at low energy is also the source of the largest difference between the local and nonlocal models, contributing to 93% of the difference at an energy of 0.01 eV. The remaining 7% comes from the $2^3\Pi_g$, $2^3\Pi_u$, and $2^3\Delta_u$ states.

The high-energy peak in the cross section is due to contributions from many resonant states. These states have potential energy curves that cross the ion potential at larger bond distances than the equilibrium distance. The cross section from some of the resonant states (such as the $1^3\Sigma_g^+$ and $1^3\Delta_g$ states) shows a smooth onset in the cross section indicating that the asymptotic limit of the state is energetically below the rise of the energy-dependent capture probability. For other states (such as the $4^3\Pi_g$ state) there is a sharp threshold where the channel becomes open for dissociation. Furthermore, for some of the resonant states (e.g., $2^1\Sigma_u^-$) there are sharp peaks in the cross section just above the thresholds. These oscillations can be interpreted as shape resonances created by tunneling through a barrier in the potential. Similar shape resonances have been observed in the cross section for other molecular systems such as HF [28].

C. Thermal rate coefficient

The thermal rate coefficient is calculated by convoluting the total cross section with the isotropic velocity distribution according to Eq. (6). Before integration, the cross section is extrapolated toward smaller energies using a function of the form $\sigma(E) = \sigma_0/E^k$. The resulting rate is shown with the thick black curve in Fig. 6 for electron temperatures ranging from 10 to 100 000 K. This rate coefficient is similar in magnitude to the majority of DR rates seen in other systems and it matches the estimates given in the classical paper by Bates [30]. At low electron temperatures (10 K $\leqslant T_e \leqslant$ 400 K) the thermal rate coefficient can be fit to the form $\alpha(T_e) = \alpha_0(300/T_e)^b$, where $\alpha_0 = 3.334 \times 10^{-8}$ cm^{3}s^{-1} and $b = 0.365$. The result of the fit is displayed with the (green) dotted curve. As can be seen the fit works only for very low temperatures since the "high-energy peak" in the cross section will cause a peak in the thermal rate coefficient centered around 5000 K.

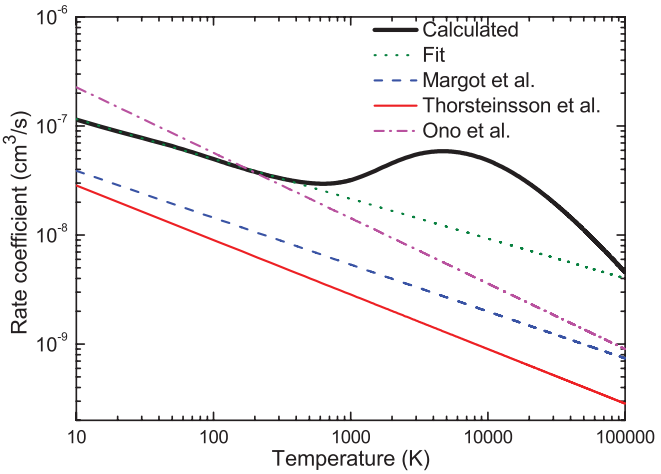

FIG. 6. (Color online) Computed thermal rate coefficient for direct DR of Cl_2^+ ($v_0 = 0$) is compared with the fit rate of the form $\alpha(T_e) = \alpha_0(300/T_e)^b$ as well as the rate coefficients assumed in the modeling of plasmas by Margot *et al*. [9], Thorsteinsson *et al*. [10], and Ono *et al*. [29].

As mentioned above the thermal rate coefficient for this reaction has never been measured nor calculated. This reaction is believed to be one of the main destruction mechanisms of the Cl_2^+ ions in chlorine etching plasmas [9]. The thermal rate coefficient for this reaction used in the modeling of the plasmas have typically been estimated using the rate coefficients for DR of other diatomic molecular ions. Usually an analytical form similar to the function we used for fitting the rate at low temperatures is applied. In Fig. 6, the temperature dependencies of some of the rate coefficients used in the literature are displayed and compared with the rate coefficient here computed. The rate coefficients from Thorsteinsson *et al*. [10] and Ono *et al*. [29] are lower than our rate for all temperatures, while the rate coefficient applied by Margot *et al*. [9] is larger than the computed rate at low temperatures and lower at higher temperatures.

D. Vibrational excited target ions

Above we have discussed the DR cross section for vibrationally relaxed ($v_0 = 0$) molecular ions. Since the Cl_2^+ ions have no permanent dipole moment, the ions will not vibrationally relax by emitting photons. For a vibrational temperature of 300 K, the Boltzmann distribution of the vibrational states of Cl_2^+ is displayed in Fig. 7. The energy eigenvalues of the vibrational states of Cl_2^+ are calculated by numerically solving the time-independent Schrödinger equation for the ionic ground state using a discrete variable representation of the Hamiltonian. It should be noted that the ground vibrational state contribute with a population of about 93% at room temperature. However, in order to examine the role of vibrationally excited ions for DR, we have also performed studies of the dynamics for ions in the $v_0 = 1$ and $v_0 = 2$ vibrational states. The cross sections for DR of Cl_2^+ in the vibrational states $v_0 = 0,1,2$ are displayed in Fig. 8. The cross sections for vibrationally excited ions is slightly higher at low energies as a result of a wider initial wave function. Also, the high-energy peak is shifted toward lower energies

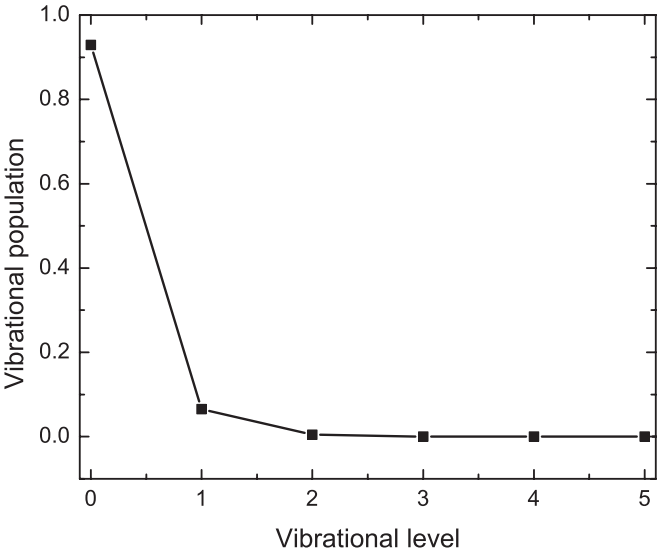

FIG. 7. Boltzmann distribution for the population of the vibrational distribution for room temperature $T = 300$ K.

as a result of the shift of the zero-point energy. The overall shape of the cross sections of the vibrationally excited ions is however very similar to the shape of the cross section for $v_0 = 0$. Also, the Boltzmann averaged cross section for a vibrational temperature of 300 K is shown in the figure. Because of the strong dominance of the ground vibrational state this cross section is very similar to the cross section for $v_0 = 0$.

The thermal rate coefficients for vibrational excited target ions are computed by numerically integrating the cross section according to Eq. (6). The computed rate coefficients for the excited vibrational states have a temperature dependence similar to the temperature dependence of the rate coefficient for $v_0 = 0$ displayed in Fig. 6 with a peak centered at higher temperatures. For low temperatures ($T_e \leqslant 400$ K) the thermal rate coefficients have been fit to the function $\alpha(T_e) = \alpha_0(300/T_e)^b$. Values of the parameters of this function

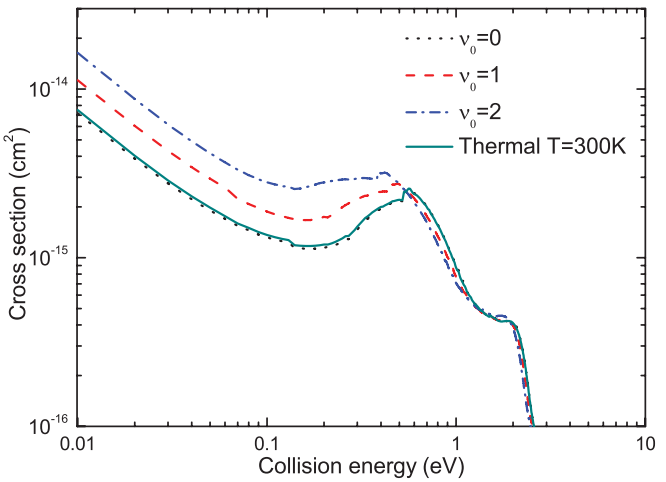

FIG. 8. (Color online) Cross section for direct DR with Cl_2^+ in the $v_0 = 0$, 1, and 2 vibrational states. The thick solid (cyan) curve shows the Boltzmann averaged cross section for a vibrational temperature of 300 K.

TABLE I. Parameters of the thermal rate coefficients for different vibrational states of $Cl_2^+(v_0)$.

v_0	α_0 (cm^3s^{-1})	b
0	3.334×10^{-8}	0.365
1	5.182×10^{-8}	0.374
2	7.509×10^{-8}	0.383

are shown in Table I. It should be noted that only at low electron temperatures these functions are able to describe the rate coefficients.

V. CONCLUSIONS

We have presented results from a theoretical study of the direct mechanism of dissociative recombination of Cl_2^+. This is a reaction that is known to be important for chlorine plasmas, however the rate for this reaction has never been studied experimentally nor theoretically before. Resonant states are computed by combining electron scattering calculations with structure calculations at the MRCI level. The cross section is calculated by solving a time-independent driven Schrödinger equation for 64 resonant states. Autoionization is included using the nonlocal approximation. A sizable cross section is found and the thermal rate coefficient is calculated. Also, the effects from vibrationally excited target ions are investigated. This paper has concentrated on the dissociative recombination process. Other reactions such as resonant vibrational excitation and dissociative excitation are of equal importance for the modeling of the chlorine high-density plasmas. Future calculations will address these reactions.

ACKNOWLEDGMENTS

Å.L. acknowledges support from The Swedish Research Council under contract No. 621-2009-3579 and A.E.O. acknowledges support from the National Science Foundation, Grant No. PHY-08-55092. M.Z. acknowledges support by the National Natural Science Foundation of China under Contract No. 10820101050 and the 973 project of the Chinese Ministry of Science and Technology under Contract No. 2010CB832900.

[1] M. Larsson and A. E. Orel, *Dissociative Recombination of Molecular Ions* (Cambridge University Press, New York, 2008).
[2] *Plasma Etching*, edited by D. M. Manos and D. L. Flamm (Academic, Boston, 1989).
[3] *Gas Lasers (Applied Atomic Collision Physics)*, edited by E. W. McDaniel and W. L. Nighan Vol. 3. (Academic, New York, 1982).
[4] R. P. Wayne, *Chemistry of Atmospheres*, 3rd ed. (OUP, New York, 2000).
[5] T. E. Graedel and P. J. Crutzen, *Chemie der Atmosphäre* (Spektrum Akademischer, Heidelberg, 1994).
[6] D. Maric, J. P. Burrows, R. Mellor, and G. K. Moortgat, J. Photochem. Photobiol., A **70**, 205 (1993).
[7] W. L. Morgan, Plasma Chem. Plasma Process. **12**, 449 (1992).
[8] L. G. Christophorou and J. K. Olthoff, J. Chem. Phys. Ref. Data **28**, 131 (1999).
[9] J. Margot, L. Stafford, J. S. Poirier, Pierre-Marc Bérubé, and M. Chaker, AIP Conf. Proc. **1125**, 166 (2009).
[10] E. G. Thorsteinsson and J. T. Gudmundsson, Plasma Sources Sci. Technol. **19**, 015001 (2010).
[11] A. D. McLean and G. S. Chandler, J. Chem. Phys. **72**, 5639 (1980).
[12] T. N. Rescigno, C. W. McCurdy, A. E. Orel, and B. H. Lengsfield III, *The Complex Kohn Variational Method in Computational Methods for Electron-Molecule Scattering*, edited by W. H. Huo and F. A. Gianturco (Plenum, New York, 1995).
[13] B. I. Schneider and T. N. Rescigno, Phys. Rev. A **37**, 3749 (1988).
[14] S. Geltman, *Topics in Atomic Collision Theory* (Academic Press, New York, 1997), p. 31.
[15] T. F. O'Malley, Phys. Rev. **150**, 14 (1966).
[16] C. W. McCurdy and J. L. Turner, J. Chem. Phys. **78**, 6773 (1983).
[17] A. E. Orel, Phys. Rev. A **62**, 020701 (2000).
[18] C. W. McCurdy, M. Baertschy, and T. N. Rescigno, J. Phys. B **37**, R137 (2004).
[19] B. Simon, Phys. Lett. A **71**, 211 (1979).
[20] C. S. Trevisan, K. Houfek, Z. Zhang, A. E. Orel, C. W. McCurdy, and T. N. Rescigno, Phys. Rev. A **71**, 052714 (2005).
[21] S. D. Peyerimhoff and R. J. Buenker, Chem. Phys. **57**, 279 (1981).
[22] D. B. Kokh, A. B. Alekseyev, and R. J. Buenker, J. Chem. Phys. **115**, 9298 (2001).
[23] J. B. Roos, Å. Larson, and A. E. Orel, Phys. Rev. A **76**, 042703 (2007).
[24] Å. Larson and A. E. Orel, Phys. Rev. A **80**, 062504 (2009).
[25] J. B. Roos, M. Larsson, Å. Larson, and A. E. Orel, Phys. Rev. A **80**, 012501 (2009).
[26] A. Giusti, J. Phys. B **13**, 3867 (1980).
[27] E. P. Wigner, Phys. Rev. **73**, 1002 (1948).
[28] J. B. Roos, Å. Larson, and A. E. Orel, Phys. Rev. A **78**, 022508 (2008).
[29] K. Ono, M. Tuda, H. Ootera, and T. Oomori, Pure Appl. Chem. **66**, 1327 (1994).
[30] D. R. Bates, Phys. Rev. **78**, 492 (1950).